<div align="center">Supporting Information</div>

Synthesizing Pd-based high entropy alloy nanoclusters for enhanced oxygen reduction

Experimental section

Synthesis of 5-Pd-HECs/C

44.13 mg of sodium tetrachloropalldate (Na_2PdCl_4), 2.16 mg of manganese acetate ($Mn(CH_3COO)_2$), 5.05 mg of iron nitrate nonahydrate (($Fe(NO_3)_3 \cdot 9H_2O$), 2.5 mg of copper acetate ($Cu(CH_3COO)_2$), and 3.11 mg of nickel acetate tetrahydrate ($Ni(CH_3COO)_2 \cdot 4H_2O$) were dissolved into 7 mL of ethanol in turn under ultrasonication for over 25 minutes. Then 44.00 mg of XC-72 carbon was added into above mixture, followed by another 15 minutes of ultrasonication to ensure uniform mixing of the metal precursors and XC-72 carbon. The obtained mixed solution was transferred to a vacuum drying oven and dried at 90°C for 2 h. Finally, the collected sample was heated at 800°C using Joule heating equipment in a hydrogen atmosphere, and the obtained sample was named as PdMnFeCuNi NCs/C (5-Pd-HECs/C). In addition, to understand the impact of the carbon supports in 5-Pd-HECs/C with different graphitization degree on ORR activity, XC-72 carbon was firstly heated at different temperatures, including 600, 800, and 1000°C, for 1 h under argon atmosphere. The obtained treated carbons were named as C-600, C-800, and C-1000, respectively. Then 5-Pd-HECs/C-600, 5-Pd-HECs/C-800, and 5-Pd-HECs/C-1000 were prepared using the same synthetic procedures of 5-Pd-HECs/C.

Synthesis of 6-Pd-HECs/C

44.13 mg of Na_2PdCl_4, 5.19 mg of $Mn(CH_3COO)_2$, 12.12 mg of $Fe(NO_3)_3 \cdot 9H_2O$, 5.45 mg of $Cu(CH_3COO)_2$, 7.47 mg of $Ni(CH_3COO)_2 \cdot 4H_2O$, and 7.47mg of cobalt acetate tetrahydrate ($Co(CH_3COO)_2 \cdot 4H_2O$) were dissolved into 10 mL of ethanol in turn under ultrasonication for over 25 minutes. Then 57.61 mg of XC-72 carbon was added into above mixture, followed by another 15 minutes of ultrasonication to ensure uniform mixing of the metal precursors and XC-72 carbon. The obtained mixed solution was transferred to a vacuum drying oven and dried at 90°C for 2 h. Finally, the

collected sample was heated at 800°C using Joule heating equipment in a hydrogen atmosphere, and the obtained sample was named as PdMnFeCuNiCo NCs/C (6-Pd-HECs/C).

Synthesis of 8-Pd-HECs/C

44.13 mg of Na_2PdCl_4, 3.7 mg of $Mn(CH_3COO)_2$, 8.65 mg of $Fe(NO_3)_3 \cdot 9H_2O$, 3.89 mg of $Cu(CH_3COO)_2$, 5.33 mg of $Ni(CH_3COO)_2 \cdot 4H_2O$, 5.33mg of $Co(CH_3COO)_2 \cdot 4H_2O$, 6.37 mg zinc nitrate hexahydrateand ($Zn(NO_3)_2 \cdot 6H_2O$), and 3.64 mg silver nitratewere ($AgNO_3$) were dissolved into 10 mL of ethanol in turn under ultrasonication for over 25 minutes. Then 60.36 mg of XC-72 carbon was added into above mixture, followed by another 15 minutes of ultrasonication to ensure uniform mixing of the metal precursors and XC-72 carbon. The obtained mixed solution was transferred to a vacuum drying oven and dried at 90°C for 2 h. Finally, the collected sample was heated at 800°C using Joule heating equipment in a hydrogen atmosphere, and the obtained sample was named as PdMnFeCuNiCoZnAg NCs/C (8-Pd-HECs/C).

Electrochemical measurements

All electrochemical tests were performed in a standard three-electrode cell equipped with a CHI760E electrochemical workstation. A graphite rod was used as the counter electrode, Hg/HgO electrode was selected as the reference electrode. A rotating disk electrode (RDE) with a diameter of 5 mm (surface area: 0.196 cm^{-2}) functions as the working electrode was. To prepare the catalyst ink, a certain amount of 5-Pd-HECs/C was added to a mixture of ethanol, deionized water, and Nafion, followed by 30 minutes of sonication. Subsequently, 15 μL of the catalyst was dropped onto the surface of the RDE for further electrochemical testing, with a Pd loading of 34.3 μg cm^{-2}. Prior to the ORR test, the alkaline electrolyte (0.1 M KOH) was saturated with oxygen by bubbling. ORR polarization curves were measured in the oxygen saturated 0.1 M KOH electrolyte under 1600 rpm at a scan rate of 5 mV s^{-1}. Durability testing was conducted in 0.1 M KOH electrolyte between 0.6 V and 1.1 V, with a scan rate of 5 mV s^{-1}. The specific activities of Pd/Pt-based catalysts were obtained by normalizing their kinetic current (i_k) to the corresponding ECSAs, while the mass activities were obtained by normalizing i_k to their Pd loadings. Additionally, current density was normalized to the geometric area of the working electrode. The kinetic current of the catalyst was calculated using the Koutecky-Levich equation: $i_k = (i_d \times i)/(i_d - i)$, where i_k, i_d, and i are the kinetic current, diffusion-limited current, and measured current, respectively.

All reported potentials in this study were converted to the reversible hydrogen electrode (RHE) scale.
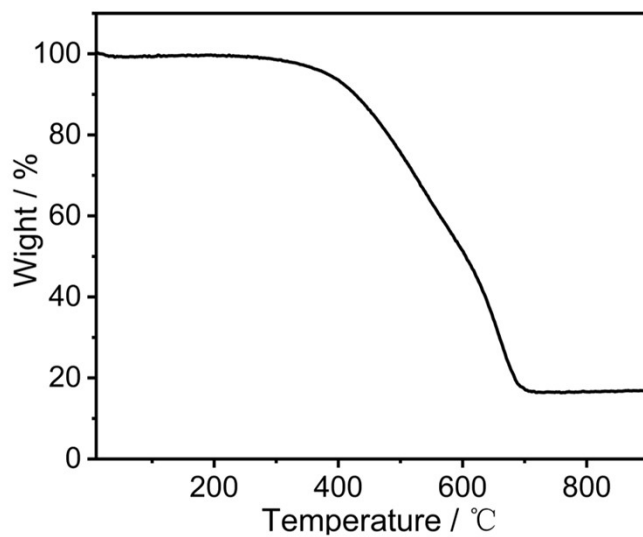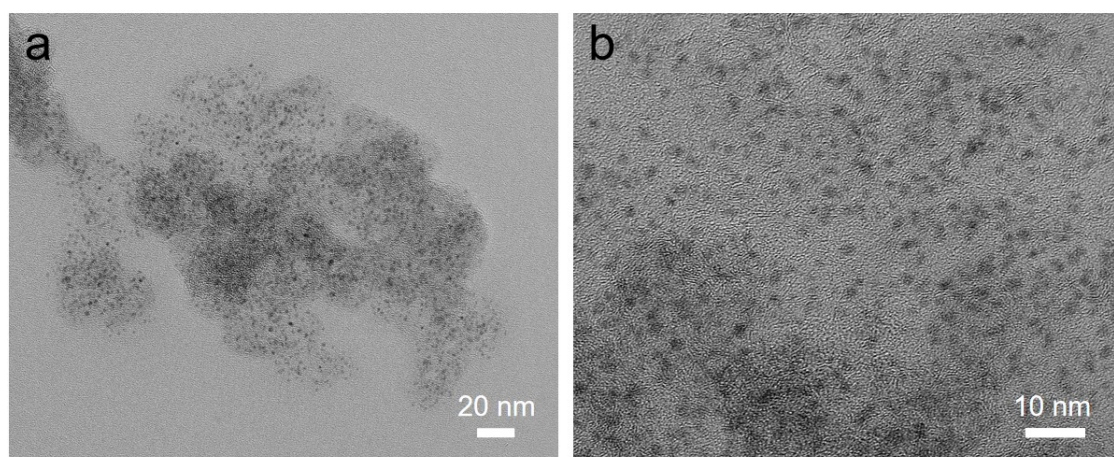

Fig. S1. TGA curve of 5-Pd-HECs/C.
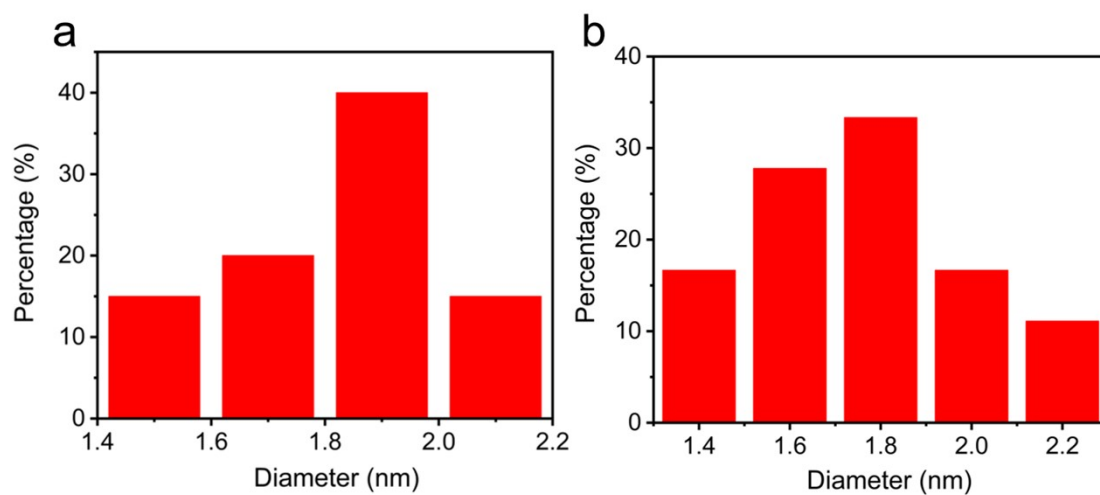

Fig. S2. TEM images of Pd-NCs/C.

Fig. S3. Crystal size histogram of (a) 6-Pd-HECs/C and (b) 8-Pd-HECs/C.
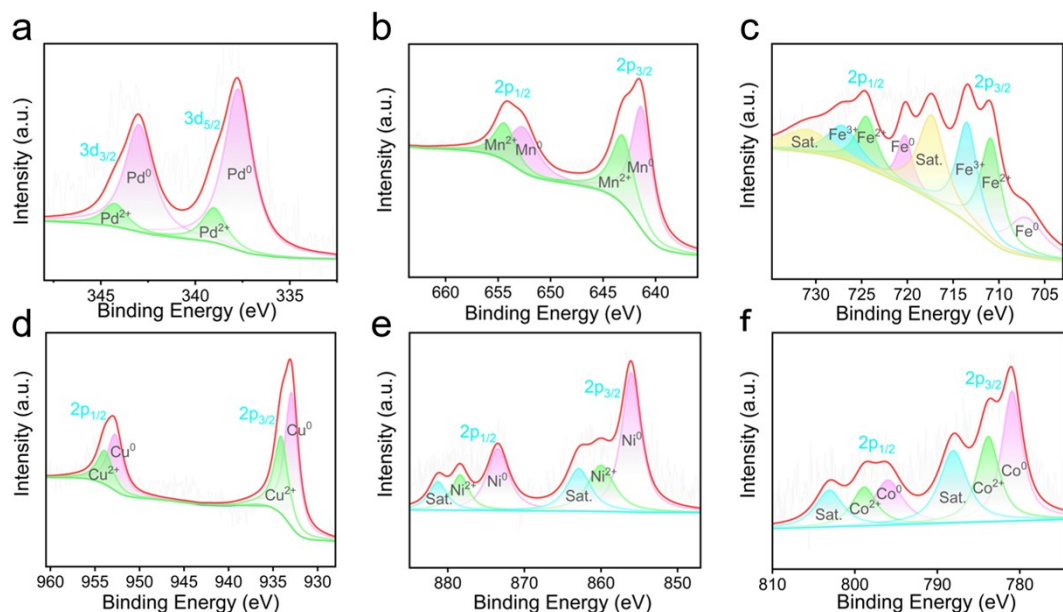

Fig. S4. XPS spectra of (a) Pd 3d, (b) Mn 2p, (c) Fe 2p, (d) Cu 2p, (e) Ni 2p and (f) Co 2p for 6-Pd-HECs/C.
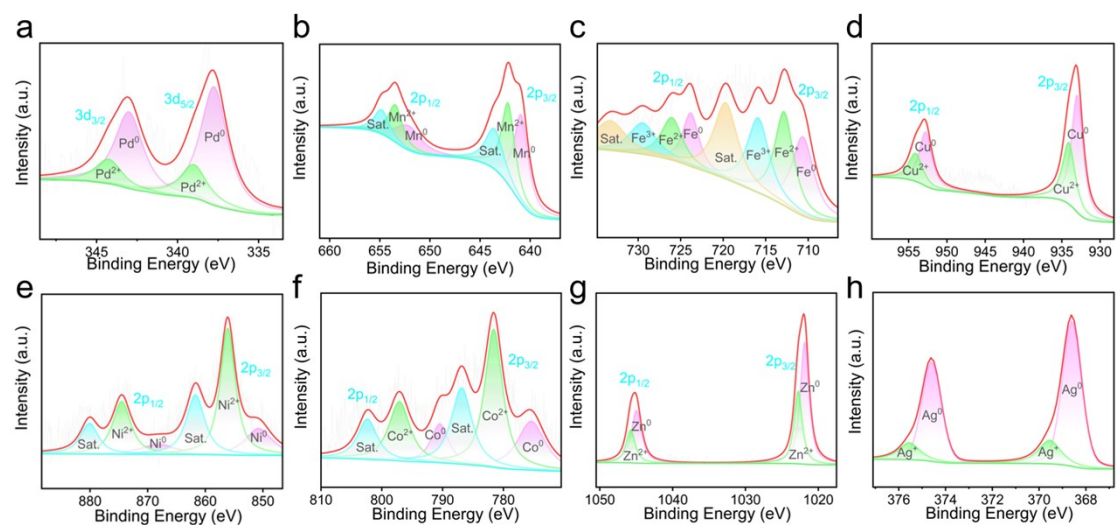

Fig. S5. XPS spectra of (a) Pd 3d, (b) Mn 2p, (c) Fe 2p, (d) Cu 2p, (e) Ni 2p, (f) Co 2p, (g) Zn 2p and (h) Ag 3d for 8-Pd-HECs/C.
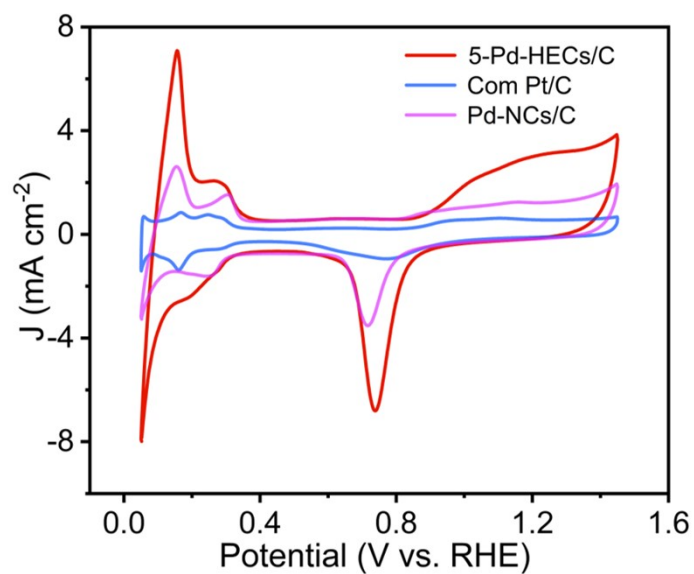
Fig. S6. CV curves of 5-Pd-HECs/C, Com Pt/C and Pd-NCs/C in 0.5 M H_2SO_4 electrolyte with the scan rate of 50 mV s^{-1}.
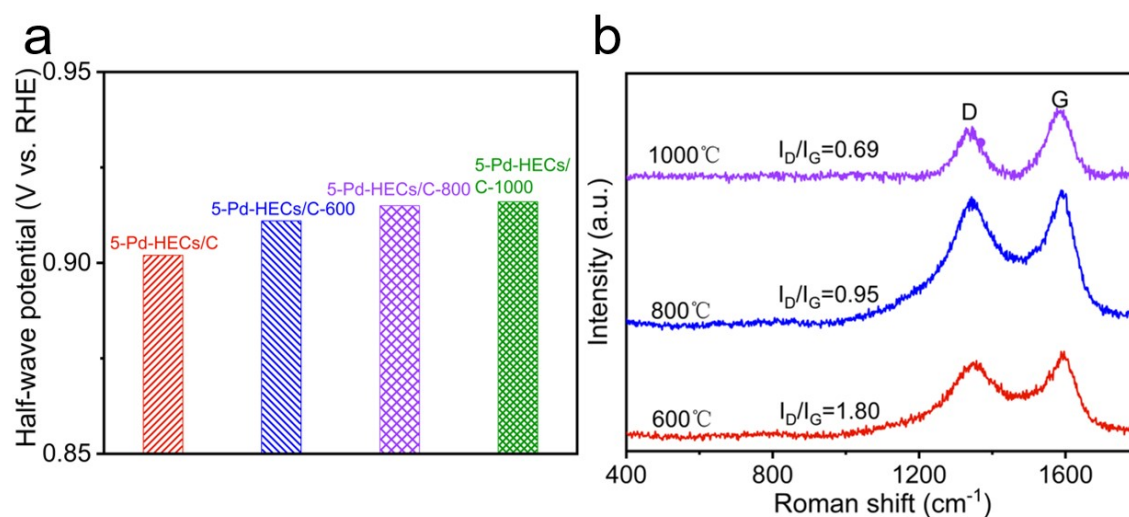

Fig. S7. (a) Half-wave potential comparisons among 5-Pd-HECs/C, 5-Pd-HECs/C-600, 5-Pd-HECs/C-800, and 5-Pd-HECs/C-1000. (b) Raman spectra of XC-72 carbon heated at 600, 800, and 1000°C for 1 h.
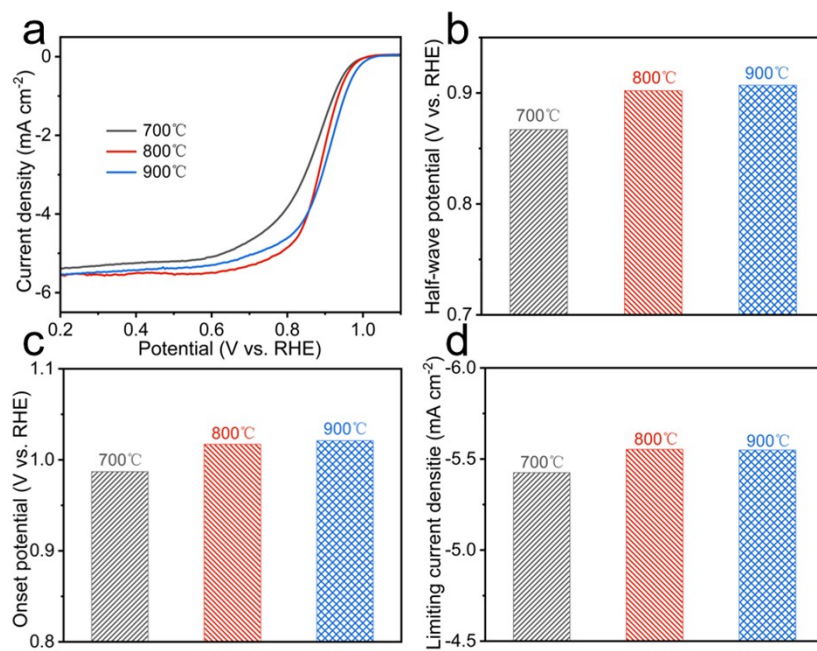
Fig. S8. Comparison of the (a) LSV curves, (b) half-wave potential, (c) onset potential, and (d) limiting current density of 5-Pd-HECs/C prepared at 700°C, 800°C, and 900°C.
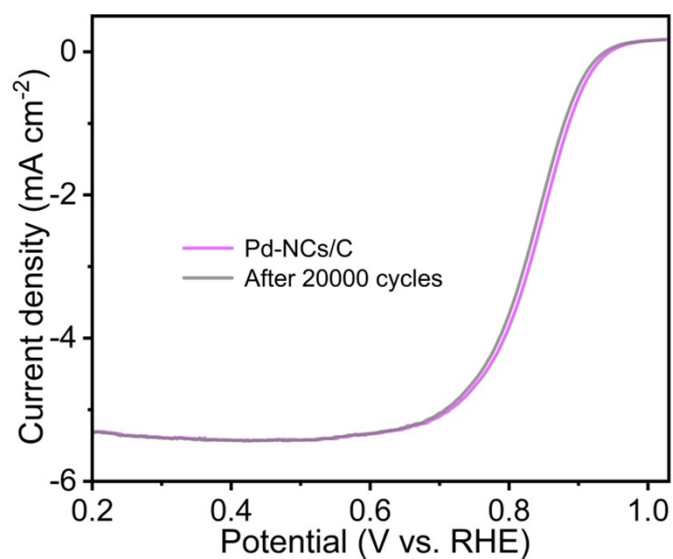

Fig. S9. LSV curves of Pd-NCs/C before and after stability testing.
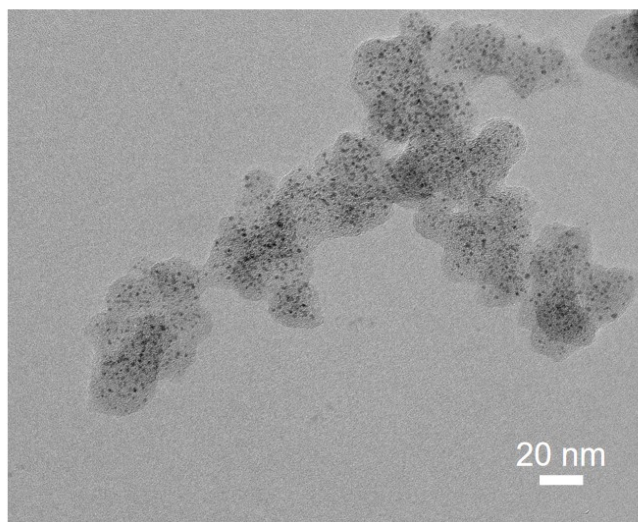
Fig. S10. TEM image of 5-Pd-HECs/C after stability testing.
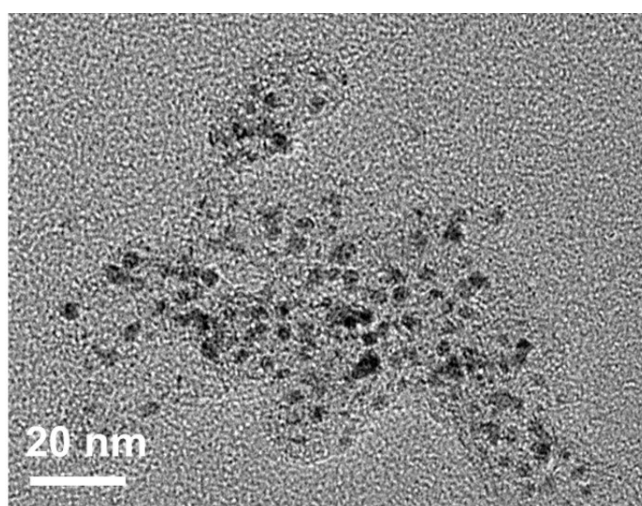

Fig. S11. TEM image of Pd-NCs/C after stability testing.
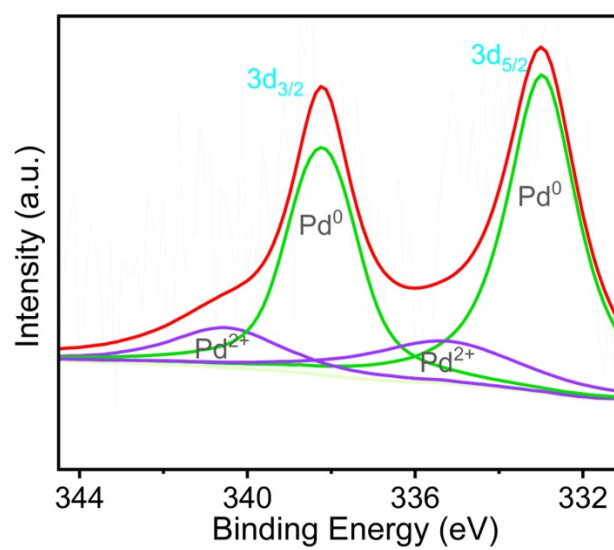

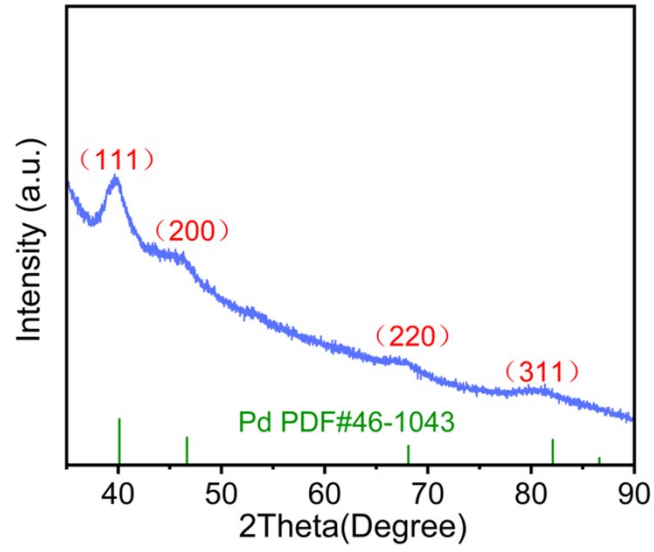Fig. S12. Pd 3d XPS spectrum of Pd-NCs/C after 20000 stability testing.

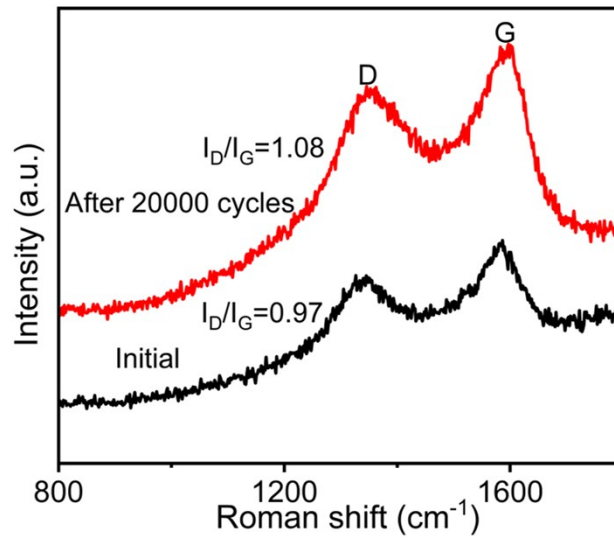Fig. S13. XRD pattern of Pd-NCs/C after 20000 stability testing.

Fig. S14. Raman spectra of Pd-NCs/C before and after 20000 stability testing.

Table S1. Comparison of catalytic behaviors of 5-Pd-HECs/C and reported various Pd-based catalysts in ORR.

Catalyst	ECSA (m^2 g^{-1}_{Pd})	Mass activity (mA mg^{-1}_{Pd})	Half-wave potentials (V)	Onset potential (V)	Limiting current density (mA cm^2)	Half-wave potential decay after stability test (mV)	Ref
5-Pd-HECs/C	113.7	993	0.902	1.017	-5.402	2	This work
PdNS/WNi/C	——	496	~0.90	~0.98	~-5.57	~15	[1]
Pd metalene/C	66.7	892	0.90	1.02	~-6.0	——	[2]
Pd@PEI-EDA	56.16	730	0.968	1.028	~-5.9	13	[3]
Pd/C$_{0.05}$	26.35	220	0.929	——	——	25	[4]
Pd$_{31}$Bi$_{12}$/C	——	950	0.92	0.97	~-6.2	——	[5]
Fe−Pd UPM	81.95	736	0.914	~0.98	~-5.6	——	[6]
AgPd120NW	——	161	0.840	~0.91	~-5.7	——	[7]
PdCu bimetallene	80.88	820	0.96	1.04	~-5.9	5	[8]
Pd$_3$Pb/Pd NSs	43.7	574	~0.91	~0.98	~-5.9	——	[9]
Pd/W$_{18}$O$_{49}$	48	216	0.875	~0.92	~-5.8	24	[10]
Pd/a-MnO$_2$	42.5	800	0.87	~0.93	——	——	[11]
Pd/MR1-SA-CaCO$_3$	41.12	610	0.892	1.085	——	——	[12]

References

[1] L. Song, Z. Liang, K. Nagamori, H. Igarashi, M. B. Vukmirovic, R. R. Adzic, K. Sasaki, Enhancing oxygen reduction performance of Pt monolayer catalysts by Pd (111) nanosheets on WNi substrates. *ACS Catalysis,* 2020, **10**(7), 4290-4298.

[2] H Yu, T. Zhou, Z. Wang, Y. Xu, X. Li, L. Wang, H. Wang, Defect-rich porous palladium metallene for enhanced alkaline oxygen reduction electrocatalysis. *Angewandte Chemie,* 2021, **133**(21), 12134-12138.

[3] Z. Wang, S. Xu, Q. Mao, K. Deng, Y. Xu, H. Wang, L. Wang, Polyethylenimine-Ethylenediamine-Induced Pd Metallene toward Alkaline Oxygen Reduction. *Inorganic Chemistry,* 2023, **62**(33), 13537-13543.

[4] L. Tong, X. Lin, J. Cai, Fu. W, X. Deng, Effect of calcium ion concentration on the ORR performance of Pd/C catalysts. *RSC advances,* 2023, **13**(51), 36373-36381.

[5] Y. Wang., A. S. Hall, Pulsed electrodeposition of metastable $Pd_{31}Bi_{12}$ nanoparticles for oxygen reduction electrocatalysis. *ACS Energy Letters,* 2019, **5**(1), 17-22.

[6] S. Huang, S. Lu, S. Gong, Q. Zhang, F. Duan, H. Zhu, M. Du, Sublayer stable Fe dopant in porous Pd metallene boosts oxygen reduction reaction. *ACS Nano,* 2021,**16**(1), 522-532.

[7] M. Lüsi, H. Erikson, H. M. Piirsoo, J. Aruväli, A. Kikas, V. Kisand, K. Tammeveski, Oxygen reduction reaction on AgPd nanocatalysts prepared by galvanic exchange. *Applied Surface Science,* 2023, 157859.

[8] Z. Wang, P. Tian, H. Zhang, K. Deng, H. Yu, Y. Xu, L. Wang, PdCu Bimetallene for Enhanced Oxygen Reduction Electrocatalysis. *Inorganic Chemistry,* 2023, **62**(14), 5622-5629.

[9] C. Tang, N. Zhang, Y. Ji, Q. Shao, Y. Li, X. Xiao, X. Huang, Fully tensile strained Pd_3Pb/Pd tetragonal nanosheets enhance oxygen reduction catalysis. *Nano Letters*, 2019, **19**(2), 1336-1342.

[10] Y. Lu, Y. Jiang, X. Gao, X. Wang, W. Chen, Strongly coupled Pd nanotetrahedron/tungsten oxide nanosheet hybrids with enhanced catalytic activity and stability as oxygen reduction electrocatalysts. *Journal of the American chemical Society*, 2014, **136**(33), 11687-11697.

[11] Y. Wang, J. Liu, H. Yuan, F. Liu, T. Hu, B. Yang, Strong Electronic Interaction between Amorphous MnO_2 Nanosheets and Ultrafine Pd Nanoparticles toward Enhanced Oxygen Reduction and Ethylene Glycol Oxidation Reactions. *Advanced Functional Materials,* 2023, 2211909.

[12] X. Deng, M. Lao, H. Zhou, J. Huang, S. Li, Y. Liang, Z. Xie, Pd Nanoparticles on Carbon Supports as Electrocatalysts for the Oxygen Reduction Reaction. *ACS Applied Nano Materials,* 2023, **6**(21), 20320-20328.